Cureus
Part of SPRINGER NATURE

Open Access Original Article

Artificial Intelligence-Based Segmentation of Local Anesthetic Spread During Ultrasound-Guided Rectus Sheath Block: An Exploratory Observational Study

Review began 09/27/2026
Review ended 10/18/2026
Published 10/29/2026

© Copyright 2026
Ono et al. This is an open access article distributed under the terms of the Creative Commons Attribution License CC-BY 4.0., which permits unrestricted use, distribution, and reproduction in any medium, provided the original author and source are credited.

DOI: 10.7759/cureus.118811

Sae Ono [1, 2], Takuya Mizukami [2], Tomoharu Shakuo [1], Ken Hirai [1, 2], Shota Tanimoto [1, 2], Yukiko Inoue [2], Ko Imamura [2], Masayoshi Kawasaki [2], Takuya Miwa [2], Seiji Mochizuki [2], Megumi Hashimoto [1], Naoki Uchida [2], Kenji Shida [1]

1. Anesthesiology, Showa Medical University Northern Yokohama Hospital, Yokohama, JPN 2. Division of Clinical Pharmacology, Showa Medical University, Tokyo, JPN

Corresponding author: Tomoharu Shakuo, tomoharu.shakuo@gmail.com

Abstract

Introduction

Ultrasound-guided rectus sheath block (RSB) requires local anesthetic spread between the posterior surface of the rectus abdominis muscle and the posterior rectus sheath. Injectate distribution is usually assessed visually, and standardized quantitative assessment methods have not yet been established. Previous artificial intelligence (AI) applications in regional anesthesia have primarily targeted anatomical structures; automatic segmentation of dynamic local anesthetic spread remains underexplored. This exploratory study aimed to develop an AI model for automatic segmentation of local anesthetic spread during RSB and evaluate its performance.

Materials and methods

This prospective, single-center observational study included 40 adults who underwent abdominal surgery and received ultrasound-guided RSB between April 2025 and February 2026. Still images were extracted at 10 frames per second from left-sided RSB videos. Cases were divided equally between training and test datasets. Experienced anesthesiologists manually segmented the local anesthetic distribution area to create manually annotated reference masks. A Mask R-CNN (region-based convolutional neural network) model implemented in Detectron2 was trained on the training dataset. Predicted masks were compared with reference masks. The primary outcome was the case-level mean Dice coefficient; secondary outcomes were case-level mean sensitivity and precision. Differences in the Dice coefficient among area groups were assessed using a linear mixed-effects model with case as a random effect, followed by pairwise comparisons of estimated marginal means with Holm adjustment.

Results

The training and test datasets contained 3,808 and 4,218 still images from 20 cases each, respectively. In the test dataset, the median case-level mean Dice coefficient, sensitivity, and precision were 0.822, 0.867, and 0.874, with interquartile ranges (IQRs) of 0.662-0.865, 0.703-0.929, and 0.796-0.911, respectively. The Dice coefficient differed significantly among area groups ($p<0.001$), with significantly higher values in the medium- and large-area groups than in the small-area group and in the large-area group than in the medium-area group after Holm adjustment.

Conclusion

The AI model demonstrated promising segmentation performance for the local anesthetic distribution area on ultrasound images obtained during RSB. These findings support the feasibility of AI-based segmentation of dynamically changing injectate spread and provide a basis for further technical and clinical investigation.

Categories: Healthcare Technology, Anesthesiology
Keywords: artificial intelligence, deep learning, image segmentation, local anesthetic spread, rectus sheath block, regional anesthesia, ultrasound imaging

Introduction

Rectus sheath block (RSB) is a regional anesthetic technique that targets the terminal muscular and anterior cutaneous branches of the thoracoabdominal nerves to provide somatic analgesia for midline incisions [1]. It is widely used for perioperative analgesia in abdominal surgery [1,2] and has been reported to reduce intraoperative and postoperative opioid consumption and postoperative pain [1,3,4]. RSB is performed by depositing local anesthetic in the fascial plane between the posterior aspect of the rectus abdominis muscle

and the posterior rectus sheath, known as the rectus sheath space. Injection outside the intended fascial plane may result in intramuscular deposition, inadequate spread, and reduced block efficacy [2,5]. Therefore, accurate deposition within the intended plane is essential [1].

During ultrasound-guided regional anesthesia, local anesthetic spread appears as a hypoechoic area and may be recognized through displacement of surrounding tissues and separation of fascial layers. However, visibility varies with the spread pattern and echogenic contrast with adjacent tissues, making the local anesthetic distribution area difficult to identify from standard ultrasound images alone [6]. A previous study used a mixture containing an ultrasound contrast agent during ultrasound-guided RSB and suggested that contrast-enhanced ultrasonography may improve visualization of local anesthetic distribution and help inform decisions regarding additional injection [6]. These findings underscore the need for objective assessment of injectate distribution during RSB. However, automatic extraction of the local anesthetic distribution area from standard ultrasound images without contrast agents remains insufficiently investigated.

Artificial intelligence (AI) applications in medicine have expanded, including clinical applications in anesthesiology [7,8]. AI-based image analysis techniques have also been applied to ultrasound-guided regional anesthesia [9]. During these procedures, operators must identify anatomical structures, the needle tip, and local anesthetic spread on ultrasound images [10]. Even among experienced anesthesiologists, anatomical identification may be imperfect, and variability in image interpretation has been reported [11]. AI-assisted systems can provide color-overlay displays of structures such as nerves, vessels, fascia, muscles, bones, pleura, and peritoneum, thereby supporting ultrasound image interpretation and potentially helping to reduce block failure and complication risk [12,13]. Segmentation models have been developed for the brachial plexus at the interscalene level and for multiple nerve block regions [14,15]. Such AI-based visualization is expected to support image interpretation and education [16,17].

Nevertheless, previous AI studies in ultrasound-guided regional anesthesia have primarily focused on anatomical structures, including nerves, vessels, fascia, and muscles. Automatic segmentation of local anesthetic spread, a dynamic procedural feature whose size and contour change throughout injection, remains insufficiently investigated. Therefore, applying AI-based image analysis to ultrasound images obtained during RSB could enable more objective assessment and quantification of injectate spread.

Accordingly, in this exploratory study, we aimed to develop an AI model for automatic segmentation of the local anesthetic distribution area on ultrasound images obtained during RSB and to evaluate its segmentation performance using manual segmentation by anesthesiologists as the reference standard. Although in the present study we focused on offline post-hoc analysis, the results can be used as an initial step toward the development of real-time intraprocedural guidance.

Materials And Methods

Study design and patients

This exploratory, prospective, single-center observational study aimed to develop an AI model for automatic segmentation of the local anesthetic distribution area on ultrasound images obtained during RSB and to evaluate its segmentation performance. Adults who underwent abdominal surgery at Showa Medical University Northern Yokohama Hospital between April 2025 and February 2026 and received ultrasound-guided RSB based on the attending anesthesiologist's clinical judgment were eligible. Ultrasound videos were recorded during RSB.

For the present analysis, cases in which 20 mL of 0.25% levobupivacaine was administered per side and the ultrasound recordings were analyzable were included. The study was conducted in accordance with the Declaration of Helsinki and approved by the institutional ethics committee (Showa Medical University Research Ethics Review Board; approval number, 2025-0196). Informed consent was obtained using an opt-out approach.

Ultrasound-guided RSB

Ultrasound-guided RSB was performed using a Sonosite ST ultrasound system (Fujifilm Medical Co., Tokyo, Japan) with a 15-6-MHz high-frequency linear transducer. The procedures were performed by anesthesiologists with varying levels of experience, ranging from those in their first year of anesthesiology practice to board-certified anesthesiologists. All blocks were performed under the supervision of an anesthesiologist experienced in ultrasound-guided RSB. The local anesthetic solution was prepared by diluting 10 mL of 0.5% levobupivacaine with 10 mL of normal saline to yield 20 mL of 0.25% levobupivacaine. A total of 20 mL was administered per side (40 mL bilaterally). A 20-gauge, 80-mm Pencan II needle (B. Braun Aesculap, Tokyo, Japan) was used. After skin disinfection, the rectus abdominis muscle was visualized in a short-axis view lateral to the umbilical level, and the posterior aspect of the rectus abdominis muscle, posterior rectus sheath, and adjacent vessels were identified. The plane between the posterior aspect of the rectus abdominis muscle and the posterior rectus sheath was defined as the target plane. The needle was advanced from medial to lateral using an in-plane technique, and its tip was

positioned in the target plane. After confirming the absence of blood on aspiration, 20 mL of 0.25% levobupivacaine was injected over approximately 20 s. Ultrasound videos spanning the entire injection period were saved in Digital Imaging and Communications in Medicine (DICOM) format. Ultrasound depth and gain were adjusted by the attending anesthesiologist according to routine clinical practice and were not standardized.

Dataset construction

We included 40 patients in the analysis. To standardize image orientation and procedural conditions, only ultrasound videos obtained during left-sided RSB were analyzed. Still images were extracted from each DICOM video at 10 frames per second, saved in Portable Network Graphics (PNG) format, and retained at a resolution of 864×1,152 pixels. After image extraction and manual segmentation, the first 20 cases for which annotation was completed were assigned to the training dataset, and the remaining 20 cases were assigned to the test dataset. All frames from a given case were retained within the same dataset. This process yielded 3,808 images in the training dataset and 4,218 images in the test dataset. No cases overlapped between the datasets.

Reference standard segmentation

Two anesthesiologists experienced in ultrasound-guided RSB annotated the cases in which they had either performed or supervised the RSB. Each case was annotated by one anesthesiologist. Before annotation, the two anesthesiologists agreed on the criteria for identifying the local anesthetic distribution area. Newly appearing hypoechoic or anechoic regions attributable to local anesthetic spread were considered the distribution area, and the target area was defined as the local anesthetic spread between the rectus abdominis muscle and the posterior rectus sheath. Structures such as the needle or muscle tissue located within the identified distribution area were not excluded from the segmented region. No independent second review or formal inter-rater reliability assessment was performed. The visible local anesthetic distribution area was manually delineated on every extracted still image using 3D Slicer (version 5.10.0; Slicer Community; https://www.slicer.org/). Pixels within each delineated contour were labeled as the local anesthetic distribution area, generating one mask per image (Figure *1*). These masks served as supervised labels for model training and as manually annotated reference masks for comparison with AI predictions in the test dataset.

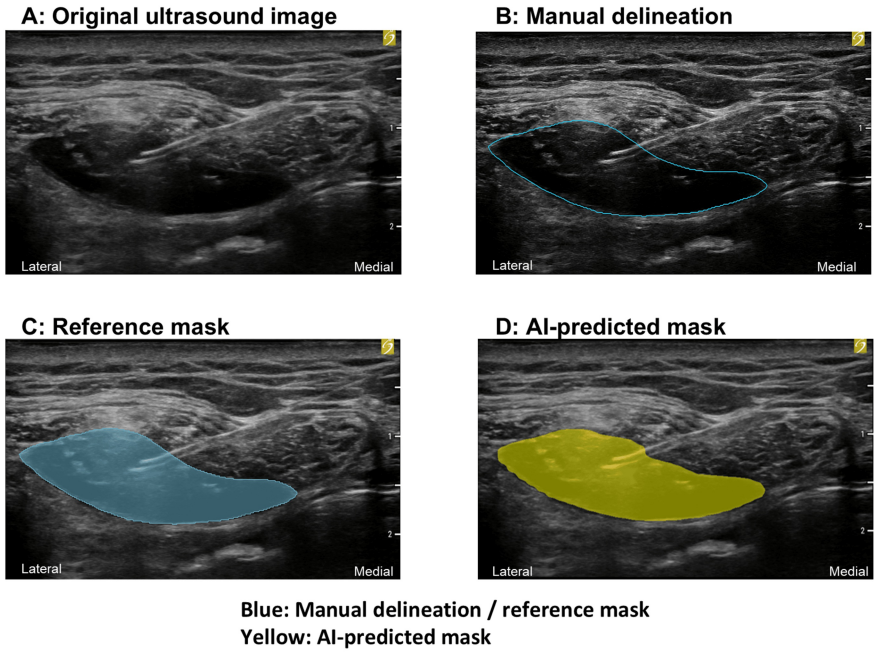


FIGURE 1: Representative ultrasound image, manual delineation, reference mask, and AI-predicted mask

(A) Original ultrasound image acquired during ultrasound-guided rectus sheath block.
(B) Manual delineation of the local anesthetic distribution area by an anesthesiologist using 3D Slicer.
(C) Reference mask generated from the manually delineated region in panel B.
(D) Local anesthetic distribution area predicted by the AI model.
The blue outline in panel B indicates the manual delineation, and the blue overlay in panel C represents the corresponding reference mask. The yellow overlay in panel D represents the AI-predicted mask.
Medial and lateral orientations are shown in each panel. AI, artificial intelligence.

AI model development

Detectron2 Framework

Detectron2 (version 0.6, Meta AI, Menlo Park, CA), an open-source framework for object detection and image segmentation [18], was used to develop the AI model. The local anesthetic distribution area was treated as a single target class, and instance segmentation was used to generate pixel-level masks for each detected region.

Model Architecture and Training

The manually created segmentation labels were converted to Common Objects in Context (COCO)-style annotations and used to train the Detectron2 model. The architecture was Mask R-CNN [19] with a ResNet-50 feature pyramid network backbone (R50-FPN), based on the COCO-InstanceSegmentation/mask_rcnn_R_50_FPN_3x.yaml configuration in the Detectron2 model zoo. Training was initialized with weights pretrained on the COCO dataset [20]. The local anesthetic distribution area was the only detection target; therefore, the number of classes was set to one. Training was performed with a batch size of 25. The initial learning rate was 0.004, and the maximum number of iterations was 2,080. After a 62-iteration warm-up, the learning rate was reduced by a factor of 0.1 at iterations 1,372 and 1,913. The workflow for dataset construction, model training, and evaluation is shown in Figure *2*.

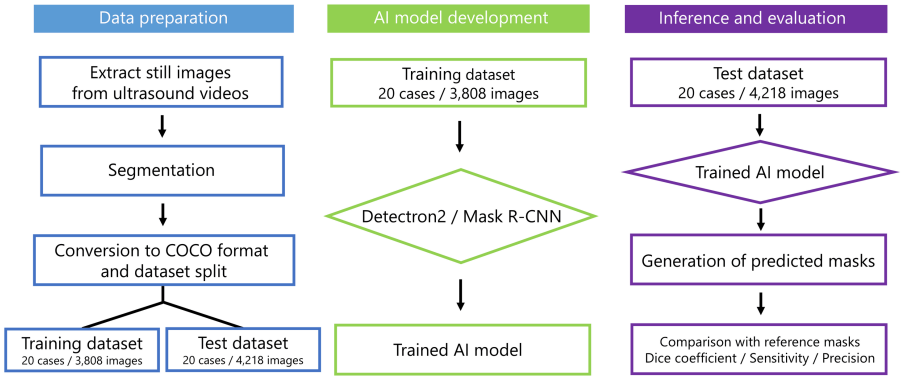


FIGURE 2: Workflow for AI model development and evaluation

Still images were extracted from ultrasound videos, manually segmented, and converted to COCO format. Cases were then assigned to either the training or test dataset at the case level, with all frames from a given case remaining within the same dataset. The training dataset was used to develop the Mask R-CNN model implemented in Detectron2, and the test dataset was used to generate the predicted masks and evaluate segmentation performance using the Dice coefficient, sensitivity, and precision. AI, artificial intelligence; COCO, Common Objects in Context; R-CNN, region-based convolutional neural network.

Model Evaluation and Outcomes

The trained model was applied to all still images from the 20 cases in the test dataset. Predicted instances with a confidence score of at least 0.5 were included in the evaluation. If no predicted instance met this threshold, the predicted mask for that frame was treated as empty.

As Mask R-CNN is an instance segmentation model, it can output multiple predicted instances within a single frame. Therefore, segmentation performance was evaluated by frame-level binary mask comparison rather than instance-level assessment. When multiple instances were predicted in a frame, their masks were merged using a pixel-wise logical OR operation to generate one binary mask. This mask was compared with the reference mask.

For performance evaluation, the Dice coefficient quantified overlap between predicted and reference masks, whereas sensitivity and precision characterized false-negative and false-positive detection, respectively. Each metric was calculated at the pixel level. Pixels predicted by the AI model as part of the local anesthetic distribution area and included in the reference mask were defined as true positives (TP). Predicted pixels outside the reference mask were defined as false positives (FP), and pixels in the reference mask that were not detected by the model were defined as false negatives (FN). The Dice coefficient, sensitivity, and precision were calculated as $2TP/(2TP+FP+FN)$, $TP/(TP+FN)$, and $TP/(TP+FP)$, respectively. When the predicted mask was empty, TP and FP were both 0; therefore, the Dice coefficient and sensitivity were set to 0. Precision was undefined in these frames and was treated as missing.

The primary outcome was the case-level mean Dice coefficient, calculated by averaging the frame-level Dice coefficients within each case. Secondary outcomes were the case-level mean sensitivity and precision. Frames with missing precision values were excluded from the calculation of mean precision.

As a supplementary analysis, all still frames in the test dataset were divided into tertiles according to the pixel area of the reference mask and classified as small-area frames (⩽42,124.67 pixels), medium-area frames (>42,124.67 to ⩽80,899 pixels), or large-area frames (>80,899 pixels). The Dice coefficient, sensitivity, and precision were summarized at the frame level for each group. Frames with missing precision values were excluded from the corresponding precision summaries. To explore changes in reference mask area as injection progressed, we identified the last frame in the small-area group and the first frame in the large-area group for each case. As videos were converted at 10 frames per second and 20 mL of local anesthetic was injected over approximately 20 s, each successive frame was assumed to represent approximately 0.1 mL of injected volume under a constant injection rate. Estimated volume was calculated by multiplying the frame order after injection began by 0.1. Cases without large-area frames were excluded from calculations involving the first large-area frame and its estimated injected volume.

Statistical analysis

The Dice coefficient and sensitivity were calculated for each still frame and then averaged within each case. Precision was averaged within each case after excluding frames with missing values. In the primary analysis, case-level values were summarized as medians and interquartile ranges. In the supplementary analysis, frame-level metrics were summarized by area group as medians and interquartile ranges. Differences in the Dice coefficient among area groups were evaluated using a linear mixed-effects model, with case included as a random effect to account for repeated frames within cases and area group included as a fixed effect. Estimated marginal means were used for post hoc pairwise comparisons, with Holm adjustment for multiple comparisons.

Continuous patient characteristics and image data are presented as mean±standard deviations, whereas categorical variables are presented as numbers (%). Statistical analyses were performed using R version 4.5.1 (R Foundation for Statistical Computing, Vienna, Austria).

Results

Patient characteristics and image data are summarized in Table *1*. Among the 40 patients, the mean age was 59.7±16.1 years, and 23 patients (57.5%) were men. Laparoscopic surgery was the most common approach and was performed in 33 patients (82.5%). The mean depth from the skin surface to the target plane was 2.0±0.6 cm, and the mean number of PNG images per case was 201±57.

Variables	Overall (n=40)	Training dataset (n=20)	Test dataset (n=20)
Age, years	59.7±16.1	58.4±16.1	61.1±16.4
Male sex	23 (57.5)	14 (70.0)	9 (45.0)
Height, cm	163.2±8.9	166.2±10.1	160.2±6.6
Weight, kg	61.4±9.3	64.0±8.3	58.7±9.7
BMI, kg/m²	22.9±3.0	23.0±2.3	22.9±3.6
ASA PS			
1	6 (15.0)	4 (20.0)	2 (10.0)
2	32 (80.0)	16 (80.0)	16 (80.0)
3	2 (5.0)	0 (0.0)	2 (10.0)
Type of surgery			
Laparoscopic surgery	33 (82.5)	18 (90.0)	15 (75.0)
Robot-assisted surgery	6 (15.0)	2 (10.0)	4 (20.0)
Open surgery	1 (2.5)	0 (0.0)	1 (5.0)
Skin-to-target plane depth, cm	2.0±0.6	2.0±0.4	2.0±0.7
Number of PNG images per case	201±57	190±57	211±51

TABLE 1: Baseline patient characteristics and image data

Values are presented as mean±standard deviation or number (%). BMI, body mass index; ASA PS, American Society of Anesthesiologists physical status; PNG, Portable Network Graphics.

In the test dataset, the median case-level mean Dice coefficient, the primary outcome, was 0.822, with an interquartile range (IQR) of 0.662-0.865. The median case-level mean sensitivity and precision, the secondary outcomes, were 0.867 (IQR, 0.703-0.929) and 0.874 (IQR, 0.796-0.911), respectively (Table *2*).

Metric	Median (IQR)
Case-level mean Dice coefficient	0.822 (0.662-0.865)
Case-level mean sensitivity	0.867 (0.703-0.929)
Case-level mean precision	0.874 (0.796-0.911)

TABLE 2: Case-level segmentation performance of the AI model in the test dataset

AI, artificial intelligence; IQR, interquartile range.

In the supplementary analysis, test-dataset frames were classified into the small-, medium-, and large-area groups based on tertiles of reference mask area, with 1,406 frames in each group. The median Dice coefficients were 0.735 (IQR, 0.416-0.851), 0.894 (IQR, 0.806-0.932), and 0.935 (IQR, 0.895-0.957) in the small-, medium-, and large-area groups, respectively. The corresponding median sensitivities were 0.844 (IQR, 0.579-0.944), 0.918 (IQR, 0.821-0.969), and 0.944 (IQR, 0.850-0.972), and the corresponding median precisions were 0.792 (IQR, 0.577-0.918), 0.903 (IQR, 0.794-0.955), and 0.952 (IQR, 0.920-0.976) (Table *3*).

Group	No. of frames	Median Dice coefficient (IQR)	Median sensitivity (IQR)	Median precision (IQR)
Small	1,406	0.735 (0.416-0.851)	0.844 (0.579-0.944)	0.792 (0.577-0.918)
Medium	1,406	0.894 (0.806-0.932)	0.918 (0.821-0.969)	0.903 (0.794-0.955)
Large	1,406	0.935 (0.895-0.957)	0.944 (0.850-0.972)	0.952 (0.920-0.976)

TABLE 3: Frame-level segmentation performance by tertile of reference mask area

IQR, interquartile range.
Small area, ≤42,124.67 pixels; medium area, >42,124.67 to ≤80,899 pixels; large area, >80,899 pixels. Precision was calculated only for frames with calculable values. The numbers of evaluable frames were 1,204 in the small-area group, 1,381 in the medium-area group, and 1,397 in the large-area group.

The linear mixed-effects model showed a significant effect of area group on the Dice coefficient ($p<0.001$). In pairwise comparisons with Holm adjustment, the Dice coefficient was higher in the medium- and large-area groups than in the small-area group and higher in the large-area group than in the medium-area group (small vs. medium, $p<0.001$; small vs. large, $p<0.001$; medium vs. large, $p=0.030$).

Small- and medium-area frames were present in all 20 cases, whereas large-area frames were present in 14 cases and absent in six. The last small-area frame occurred a mean of 72 frames after injection began across all 20 cases. The first large-area frame occurred a mean of 111 frames after injection began among the 14 applicable cases. Under the constant-rate assumption, these time points corresponded to estimated injected volumes of approximately 7.2 mL and 11.1 mL, respectively.

Discussion

In this exploratory study, we developed an AI model to automatically segment the local anesthetic distribution area on ultrasound images obtained during ultrasound-guided RSB. Evaluation using 4,218 still images from 20 test cases yielded a median case-level mean Dice coefficient of 0.822, suggesting promising segmentation performance.

A previous study of brachial plexus segmentation at the interscalene level reported a mean Dice coefficient of 0.748±0.190 and described a value near 0.75 as a benchmark for good overlap [14]. Another study segmenting nerve regions across multiple nerve block sites reported that R2U-Net achieved the highest performance among the evaluated models, with a mean Dice score of 0.7619 across all target regions [15]. The median case-level mean Dice coefficient in the present study was similar to or higher than those reported in these previous studies. However, direct comparisons should be interpreted cautiously because the target structures, model architectures, and imaging conditions differed.

In addition to the Dice coefficient, we evaluated sensitivity and precision. The Dice coefficient measures the overlap between the predicted and reference masks, whereas sensitivity and precision reflect false-negative and false-positive tendencies, respectively. These secondary outcomes were relatively high, suggesting that

the model achieved reasonably balanced performance in detecting the local anesthetic distribution area.

RSB provides analgesia to the anterior midline abdominal wall by depositing local anesthetic between the posterior aspect of the rectus abdominis muscle and the posterior rectus sheath. Because sensory blockade depends partly on injectate spread within this fascial plane [1], assessment of injectate distribution is an important element in evaluating procedural quality. Contrast-enhanced ultrasonography has been reported to improve visualization of local anesthetic distribution during RSB [6]. The present exploratory study applied AI-based segmentation to standard ultrasound images. After further technical and clinical validation, automatic segmentation could support objective recording of the area, shape, and temporal evolution of injectate spread rather than relying solely on visual judgment. Such information may eventually assist intraprocedural interpretation, education, and standardized documentation.

Recent AI research in ultrasound-guided regional anesthesia has focused mainly on the automatic identification and segmentation of anatomical structures [12-15], with potential educational applications for novice training and instructor support [16,17,21]. AI-assisted color overlays may help operators recognize anatomy and reduce the risk of block failure and complications [12,13]. Previous segmentation studies have targeted nerve regions at the interscalene level and across multiple block sites [14,15], suggesting potential contributions to improved clinical and educational quality [15]. A key novelty of the present study is its focus on the temporally changing local anesthetic distribution area rather than anatomical structures such as nerves, vessels, fascia, and muscle layers. We demonstrated that an AI model can automatically extract the injectate distribution area from ultrasound images obtained during RSB. We used Mask R-CNN with an R50-FPN backbone, implemented in Detectron2, to extract the local anesthetic distribution area. Detectron2 provides standardized implementations for object detection and image segmentation, facilitating model development and reproducibility. Mask R-CNN simultaneously detects target regions and estimates pixel-level masks [19], making it suitable for characterizing the area and shape of injectate distribution within individual frames. However, because Mask R-CNN processes each frame independently, the present model does not explicitly use the temporal continuity between successive video frames. The mean inference time was 54.51±1.97 ms per frame, measured across all frames from the 20 test cases using an NVIDIA A100-SXM4-80GB GPU. Although this provides an initial estimate of computational performance, further studies evaluating hardware requirements, temporal stability across consecutive frames, and integration into the ultrasound workflow are needed to assess the feasibility of real-time use. In clinical implementation, model performance may be influenced by operator-dependent factors such as probe handling, needle trajectory, injection technique, and level of experience, and further studies are needed to evaluate its robustness across different operators.

In the supplementary analysis, frames with larger reference masks had higher Dice coefficients, with the highest values observed in the large-area group. Across all 20 cases, the last small-area frame corresponded to an estimated injected volume of approximately 7.2 mL. In contrast, among the 14 cases with large-area frames, the first large-area frame corresponded to approximately 11.1 mL. This pattern likely reflects greater visibility of the expanding local anesthetic distribution area as injection progressed, making segmentation by the AI model easier. However, the estimated volumes were calculated assuming a constant injection rate, and six cases had no large-area frames. Performance differences may therefore reflect not only injected volume but also spread pattern, image quality, and imaging conditions. Moreover, contour deviations have a proportionally smaller effect on overlap metrics when the target region is larger. Because ultrasound imaging depth was not standardized, reference-mask area measured in pixels does not directly correspond to the physical area of local anesthetic spread across patients. Therefore, the area-stratified analysis should be interpreted as an assessment of segmentation performance according to target size within the image rather than as a comparison of the physical extent of injectate spread. Improving performance during early injection and in cases where visible spread remains limited despite sufficient injection volume is an important objective for future model development.

This study should be interpreted in light of several limitations. First, this was a single-center exploratory study of 40 cases, which limits generalizability. Second, the training and test datasets were obtained at the same institution, and we did not perform external validation. Third, the procedural and imaging conditions reflected the practice at a single institution. An 80-mm block needle was selected to provide sufficient length for an in-plane approach from a medial puncture site near the umbilicus toward the lateral aspect of the posterior rectus sheath. Only one ultrasound system was used; performance across devices and acquisition settings remains unknown. Although the analysis pipeline may be transferable to other Digital Imaging and Communications in Medicine (DICOM)-formatted videos, this possibility requires direct testing. Fourth, no separate internal validation dataset was established, limiting hyperparameter optimization and formal assessment of overfitting. Fifth, no cases in which local anesthetic failed to reach the intended target plane because of unintended intramuscular or intraperitoneal injection were included in the dataset. Therefore, the ability of the model to distinguish appropriate spread within the intended target plane from unintended intramuscular or intraperitoneal injection has not been evaluated. Future studies should include such erroneous injection patterns to assess the model's ability to distinguish appropriate from inappropriate injectate spread. A key strength and novel aspect of this study is the development of an automatic segmentation model for local anesthetic spread using real-world RSB videos and anesthesiologist-generated masks across 8,026 images. The area-stratified supplementary analysis identified conditions under which performance was stronger or weaker. These findings provide an initial basis for multicenter external

validation, prospective real-time evaluation, and investigation of whether segmentation outputs correlate with block quality or clinical outcomes.

Conclusions

This exploratory study developed an instance segmentation model for automatic extraction of the local anesthetic distribution area from ultrasound images obtained during RSB. The model showed promising segmentation performance when evaluated against manual segmentation. These findings support the feasibility of AI-based segmentation of dynamically changing injectate spread and provide a basis for further technical and clinical investigation.

Additional Information

Author Contributions

All authors have reviewed the final version to be published and agreed to be accountable for all aspects of the work.

Concept and design: Sae Ono, Takuya Mizukami, Tomoharu Shakuo, Ken Hirai, Shota Tanimoto

Acquisition, analysis, or interpretation of data: Sae Ono, Ken Hirai, Shota Tanimoto, Yukiko Inoue, Ko Imamura, Masayoshi Kawasaki, Seiji Mochizuki, Takuya Miwa, Megumi Hashimoto, Naoki Uchida, Kenji Shida

Drafting of the manuscript: Sae Ono

Critical review of the manuscript for important intellectual content: Takuya Mizukami, Tomoharu Shakuo, Ken Hirai, Shota Tanimoto, Yukiko Inoue, Ko Imamura, Masayoshi Kawasaki, Seiji Mochizuki, Takuya Miwa, Megumi Hashimoto, Naoki Uchida, Kenji Shida

Supervision: Takuya Mizukami, Tomoharu Shakuo, Naoki Uchida, Kenji Shida

Disclosures

Human subjects: Informed consent for treatment and open access publication was obtained or waived by all participants in this study. Showa Medical University Research Ethics Review Board issued approval 2025-0196. **Animal subjects:** All authors have confirmed that this study did not involve animal subjects or tissue. **Conflicts of interest:** In compliance with the ICMJE uniform disclosure form, all authors declare the following: **Payment/services info:** All authors have declared that no financial support was received from any organization for the submitted work. **Financial relationships:** All authors have declared that they have no financial relationships at present or within the previous three years with any organizations that might have an interest in the submitted work. **Other relationships:** All authors have declared that there are no other relationships or activities that could appear to have influenced the submitted work.

Acknowledgements

The authors thank Editage for English language editing.

References

1. Chin KJ, McDonnell JG, Carvalho B, Sharkey A, Pawa A, Gadsden J: Essentials of our current understanding: abdominal wall blocks. Reg Anesth Pain Med. 2017, 42:133-83. 10.1097/AAP.0000000000000545
2. Crosbie EJ, Massiah NS, Achiampong JY, Dolling S, Slade RJ: The surgical rectus sheath block for post-operative analgesia: a modern approach to an established technique. Eur J Obstet Gynecol Reprod Biol. 2012, 160:196-200. 10.1016/j.ejogrb.2011.10.015
3. Bashandy GM, Elkholy AH: Reducing postoperative opioid consumption by adding an ultrasound-guided rectus sheath block to multimodal analgesia for abdominal cancer surgery with midline incision. Anesth Pain Med. 2014, 4:e18263. 10.5812/aapm.18263
4. Jeffries SD, Harutyunyan R, Morse J, Hemmerling TM: Investigation into the clinical performance of rectus sheath block in reducing postoperative pain following surgical intervention: a systematic review and meta-analysis of randomised controlled trials. Indian J Anaesth. 2024, 68:142-52. 10.4103/ija.ija_1099_23
5. Manassero A, Bossolasco M, Meineri M, Ugues S, Liarou C, Bertolaccini L: Spread patterns and effectiveness for surgery after ultrasound-guided rectus sheath block in adult day-case patients scheduled for umbilical hernia repair. J Anaesthesiol Clin Pharmacol. 2015, 31:349-53. 10.4103/0970-9185.161671
6. Onishi E, Saito K, Kumagai M, Oba R, Murakami T, Sugino S, Yamauchi M: Evaluation of contrast-enhanced ultrasonography with Sonazoid(®) in visualization of local anesthetic distribution in rectus sheath block: a prospective, clinical study. J Anesth. 2022, 36:405-12. 10.1007/s00540-022-03063-6
7. Hashimoto DA, Witkowski E, Gao L, Meireles O, Rosman G: Artificial intelligence in anesthesiology: current techniques, clinical applications, and limitations. Anesthesiology. 2020, 132:379-94. 10.1097/ALN.0000000000002960
8. Lopes S, Rocha G, Guimarães-Pereira L: Artificial intelligence and its clinical application in anesthesiology:

a systematic review. J Clin Monit Comput. 2024, 38:247-59. 10.1007/s10877-023-01088-0
9. Viderman D, Dossov M, Seitenov S, Lee MH: Artificial intelligence in ultrasound-guided regional anesthesia: a scoping review. Front Med (Lausanne). 2022, 9:994805. 10.3389/fmed.2022.994805
10. Sites BD, Chan VW, Neal JM, Weller R, Grau T, Koscielniak-Nielsen ZJ, Ivani G: The American Society of Regional Anesthesia and Pain Medicine and the European Society Of Regional Anaesthesia and Pain Therapy Joint Committee recommendations for education and training in ultrasound-guided regional anesthesia. Reg Anesth Pain Med. 2009, 34:40-6. 10.1097/AAP.0b013e3181926779
11. Bowness J, Varsou O, Turbitt L, Burkett-St Laurent D: Identifying anatomical structures on ultrasound: assistive artificial intelligence in ultrasound-guided regional anesthesia. Clin Anat. 2021, 34:802-9. 10.1002/ca.23742
12. Bowness JS, El-Boghdadly K, Woodworth G, Noble JA, Higham H, Burckett-St Laurent D: Exploring the utility of assistive artificial intelligence for ultrasound scanning in regional anesthesia. Reg Anesth Pain Med. 2022, 47:375-9. 10.1136/rapm-2021-103368
13. Bowness JS, Burckett-St Laurent D, Hernandez N, et al.: Assistive artificial intelligence for ultrasound image interpretation in regional anaesthesia: an external validation study. Br J Anaesth. 2023, 130:217-25. 10.1016/j.bja.2022.06.031
14. Xi Y, Chong H, Zhou Y, Zhu F, Yao Y, Wang G: Convolutional neural network for brachial plexus segmentation at the interscalene level. BMC Anesthesiol. 2024, 24:17. 10.1186/s12871-024-02402-2
15. Pelletier ED, Jeffries SD, Suissa N, et al.: From consensus to standardization: evaluating deep learning for nerve block segmentation in ultrasound imaging. A A Pract. 2025, 19:e02040. 10.1213/XAA.0000000000002040
16. Balavenkatasubramanian J, Kumar S, Sanjayan RD: Artificial intelligence in regional anaesthesia . Indian J Anaesth. 2024, 68:100-4. 10.4103/ija.ija_1274_23
17. Xu FW, Choo AM, Ting PL, Ong SJ, Khoo D: Leveraging AI in postgraduate medical education for rapid skill acquisition in ultrasound-guided procedural techniques. J Imaging. 2023, 9:225. 10.3390/jimaging9100225
18. Meta AI: Detectron2 . Accessed: August 26, 2026: https://ai.meta.com/tools/detectron2/.
19. He K, Gkioxari G, Dollár P, Girshick R: Mask R-CNN . 2017 IEEE International Conference on Computer Vision (ICCV). 2017, 2980-8.
20. Lin TY, Maire M, Belongie S, et al.: Microsoft COCO: common objects in context . Computer Vision - ECCV 2014. Fleet D, Pajdla T, Schiele B, Tuytelaars T (ed): Springer, Cham; 2014. 8693:740-55. 10.1007/978-3-319-10602-1_48
21. Gungor I, Gunaydin B, Oktar SO, Buyukgebiz BM, Bagcaz S, Ozdemir MG, Inan G: A real-time anatomy ıdentification via tool based on artificial ıntelligence for ultrasound-guided peripheral nerve block procedures: an accuracy study. J Anesth. 2021, 35:591-4. 10.1007/s00540-021-02947-3